RESEARCH ARTICLE

Key Points:
- Saturn Z-mode intensity is binned in r, latitude, and local time
- Parametric fits of intensity versus frequency, r, and latitude determined
- Z-mode could supplement chorus to accelerate electrons

Survey of Saturn *Z*-mode emission

J. D. Menietti[1], T. F. Averkamp[1], S.-Y. Ye[1], R. B. Horne[2], E. E. Woodfield[2], Y. Y. Shprits[3,4], D. A. Gurnett[1], A. M. Persoon[1], and J.-E. Wahlund[5]

[1]Department of Physics and Astronomy, University of Iowa, Iowa City, Iowa, USA, [2]British Antarctic Survey, Cambridge, UK, [3]Department of Earth and Space Sciences, University of California, Los Angeles, California, USA, [4]Department of Earth, Atmospheric, and Planetary Sciences, MIT, Cambridge, Massachusetts, USA, [5]Swedish Institute of Space Physics, Uppsala, Sweden

Abstract Because of the role of *Z*-mode emission in the diffusive scattering and resonant acceleration of electrons, we conduct a survey of intensity in the Saturn inner magnetosphere. *Z* mode is primarily observed as "5 kHz" narrowband emission in the lower density regions where the ratio of cyclotron to plasma frequency, $f_c/f_p > 1$ to which we limit this study. This occurs at Saturn along the inner edge of the Enceladus torus near the equator and at higher latitudes. We present profiles and parametric fits of intensity as a function of frequency, radius, latitude, and local time. The magnetic field intensity levels are lower than chorus, but the electric field intensities are comparable. We conclude that *Z*-mode wave-particle interactions may make a significant contribution to electron acceleration in the inner magnetosphere of Saturn, supplementing acceleration produced by chorus emission.

1. Introduction

Z mode is electromagnetic emission that lies in the frequency range $f_z < f < f_{uhr}$, where $f_z = -f_c/2 + \sqrt{(f_c/2)^2 + f_p^2}$ (cutoff frequency) and $f_{uhr} = \sqrt{f_c^2 + f_p^2}$ (upper hybrid resonance), where f_c and f_p are the cyclotron and plasma frequencies, respectively. *Z* mode can occur at higher frequencies than whistler mode chorus emission, and both emissions have a cyclotron resonance [*Benson et al.*, 2006]. *Z* mode is known to be an important contributor to pitch angle, energy, and momentum diffusive scattering of electrons [cf. *Horne and Thorne*, 1998; *Glauert and Horne*, 2005; *Albert*, 2007; *Xiao et al.*, 2012]. Recently, *Gu et al.* [2013] computed the bounce-averaged diffusion coefficients for *Z*-mode emission observed near the inner edge of the Enceladus plasma torus. These authors found that *Z* mode observed near 5 kHz can cause resonant scattering of electrons from a few MeV to tens of MeV. At Saturn, *Z*-mode emission is often observed as a component of narrowband (NB) emission if it occurs for $f < f_c$, especially when $f_p/f_c < 1$ [*Farrell et al.*, 2005; *Ye et al.*, 2010]. Narrowband emission at Saturn is typically observed as "5 kHz" and "20 kHz" bands [*Ye et al.*, 2009]. Both the 5 kHz and the 20 kHz bands are observed as left-hand ordinary mode when observed at $r \gtrsim 7\ R_s$ [*Ye et al.*, 2009], but can be a mixture of ordinary (*O*) and *Z* mode in the region inside the Enceladus torus [*Ye et al.*, 2010; *Gu et al.*, 2013]. The 5 kHz NB emission in this region appears to be dominantly *Z* mode.

Following up on an earlier study of whistler mode chorus and *Z*-mode emission at Jupiter and Saturn [*Menietti et al.*, 2012], and a more comprehensive survey of chorus at Saturn [*Menietti et al.*, 2014] in this paper we survey the *Z*-mode intensities near 5 kHz in the region inside the inner edge of the Enceladus torus both near the equator and at higher latitudes. Due to the more complex nature of the emissions at higher frequency (20 kHz NB emission), we have not included them in this survey. The 5 kHz NB emission is generally more intense than 20 kHz NB emission. We provide parametric fits of the *Z*-mode intensity as function of frequency, radius, latitude, and local time in the Saturn magnetosphere. The results are valuable for diffusive as well as nonlinear studies of *Z*-mode resonant interactions with electrons at Saturn.

2. Observational Examples

In Figure 1 we show an example of NB emission observed by the Cassini radio and plasma wave instrument (RPWS) near and inside the Enceladus torus in both the 5 kHz and 20 kHz bands. As stated in *Persoon et al.* [2013], the Enceladus plasma torus has a broad density peak in the range 4 to 5 R_s. From this peak the
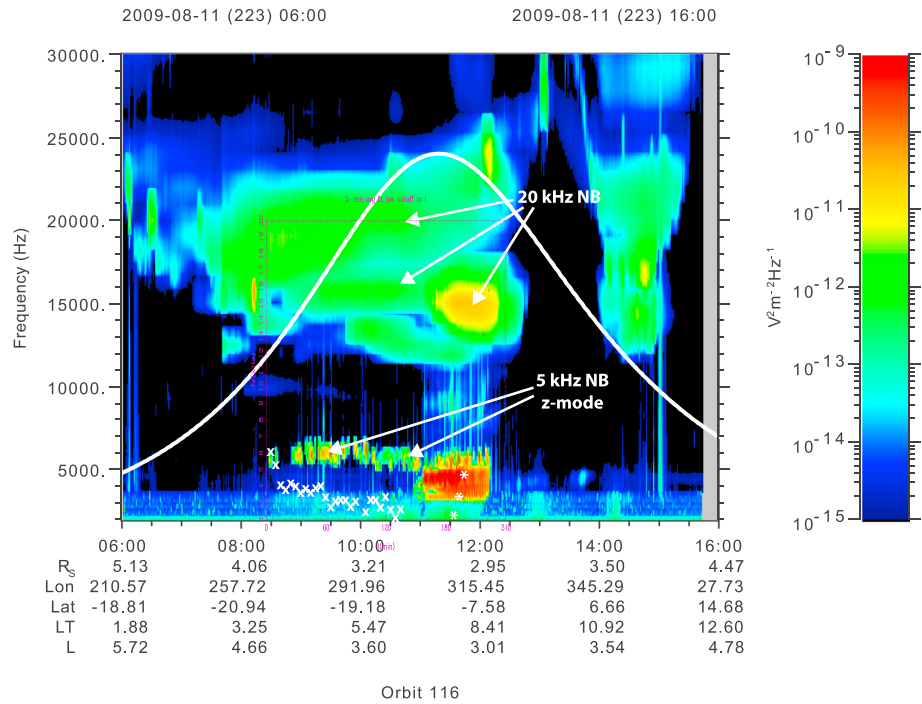
Figure 1. Frequency-time spectrogram of the electric field spectral density for a portion of day 223 of 2009. Moderate to strong electric field intensity 5 kHz emission is seen in a band from ~5 kHz to ~7 kHz at $08{:}25 < t \lesssim 11{:}00$, and most intense emission seen in the time interval ~11:00 to ~12:15 with an expanded bandwidth ~3 kHz to ~6 kHz. The value of f_z determined from Langmuir Probe data is plotted as x, while the values determined from the density model are plotted with "asterisk," The emission above 10 kHz (20 kHz NB) is generally less intense and more diffuse. Here this emission is seen to traverse the cyclotron frequency (white line), indicating a significant component of ordinary (O) mode, because Z mode cannot propagate above ~f_c (for $f_p/f_c \ll 1$).

radial density profile falls off both inward ($r^{4.0}$) and outward ($r^{-4.8}$) and the density decreases in latitude with a scale height dependence within about 8° latitude (see Figure 4 and equations (1) and (2) of *Persoon et al.* [2013]. The Cassini spacecraft is in a high-inclination orbit at this time and traverses the equator from southern to northern latitudes on 2009/223, near 13:00, having approached to within 3 R_s of Saturn. In Figure 1 moderate to strong electric field intensity 5 kHz emission is seen in a band from ~5 kHz to ~7 kHz at $08{:}25 < t < {\sim}11{:}00$, with the most intense emission seen in the time interval ~11:00 to ~12:15 with an expanded bandwidth ~3 kHz to ~6 kHz. At higher latitudes the density falls off rapidly outside the Enceladus torus. Throughout the observation of the 5 kHz Z-mode emission, $f < f_c$ and $f_p/f_c < 1$. Data from the Langmuir Probe (a Cassini instrument described later) are available for the time interval $t < 10{:}56$, where the measured electron density $n_e < 1 \, \mathrm{cm}^{-3}$, $f_p < 8$ kHz. We plot the lower frequency cutoff, f_z, with the symbol, "x" in Figure 1. The values of f_p obtained from the Langmuir Probe data drop below 2 kHz after ~10:40. The last points shown in asterisks indicate f_z obtained from the model electron density, which we must use after 10:56. These values range from ~0.3 cm^{-3} to ~1.3 cm^{-3} ($f_z \sim 3.3$ kHz) for the time interval $10{:}56 < t < 11{:}39$, after which it increases rapidly up to ~8 cm^{-3} ($f_z \sim 15.8$ kHz) near 12:10. The density measurements of the model are statistical and may not represent the actual densities at the time of the measurement, but if correct, indicate that the emissions are not Z mode for $t > {\sim}11{:}49$ and may be primarily electrostatic. The emission above 10 kHz (20 kHz NB) is generally less intense and not as bursty and is often seen to traverse the cyclotron frequency (white line), indicating a significant component of ordinary (O) mode, because Z-mode emission cannot propagate at $f > f_{uh} \sim f_c$ (for $f_p \ll f_c$). The magnetic search coils on the Cassini instrument have a relatively high noise level, and the magnetic component of the Z-mode emission is seldom observed [cf. *Ye et al.*, 2010]. For this particular example, there is a weak magnetic signal from ~11:00 to ~12:00 in the frequency range ~4 kHz $< f \lesssim 5$ kHz. Because of these typically weak or missing magnetic components, our study utilizes the electric field observations of Z mode. It is
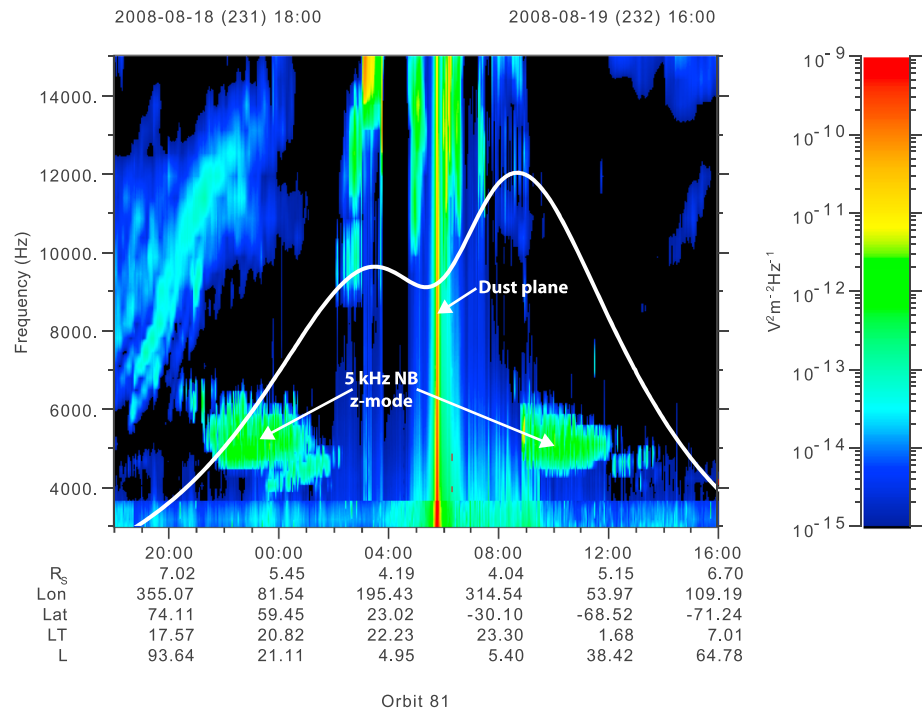
Figure 2. Z-mode emission observed on 2008 days 231 and 232 while Cassini was in another high-inclination orbit. Here the Z mode is observed near the inner edge of the torus at somewhat larger radial distances compared to Figure 1, but at higher latitudes where the densities are low and $f_p/f_c \ll 1$. The crossing of the equatorial dust plane is indicated.

important to point out that the Z-mode electric field intensity levels are comparable to the electric field intensities of Saturn chorus emissions, even though the magnetic field intensities are much weaker.

In Figure 2 we show an example of Z-mode emission observed in 2008 days 231 and 232 while Cassini was in another high-inclination orbit. We indicate the crossing of the equatorial dust plane in Figure 2. The Z mode is observed near the inner edge of the torus at somewhat larger radial distances compared to Figure 1, but at higher latitudes where the densities remain low and $f_p/f_c < 1$ and f_z is always less than the lowest frequency of the emission labeled as Z mode. For this pass, all densities were obtained from the Langmuir Probe data. The 5 kHz emission at higher latitudes is generally less intense than emissions nearer the equator.

3. Methodology

We have conducted a search of the Cassini radio and plasma wave instrument (RPWS) low rate data for 5 kHz narrowband emission. We have avoided the 20 kHz NB emission in this study because it often contains a mixture of ordinary (O) mode as well as Z mode when observed near the inner edge of the torus, whereas the 5 kHz emission appears to be predominately Z mode. The morphology of the emission is typical of that seen in Figures 1 and 2. For each episode of Z mode we record the frequency and time range.

The general scheme for conducting the Z-mode survey is similar to that used to conduct the survey of chorus [cf. *Menietti et al.*, 2014]. We introduce spatial bins in radial distance, local time (LT), and latitude (λ). Due to the small magnetic field tilt relative to the spin axis at Saturn, we have equated the magnetic local time to the local time. The survey of Saturn Z-mode emission differs from the survey of Saturn chorus, which was sampled using a computer code subject to sampling constraints. Z-mode emission is not so easily identified in this manner due to various mixing of Z-mode with O-mode emissions and the superposition of electrostatic emissions. Z mode was identified by eye using its narrowband morphology and frequency range. The time intervals of the Z-mode emission from spectrograms of the data were limited to orbits for $r < 8 \, R_s$ and that crossed the equator inside of L = 4.5. Wave polarization spectrograms were also analyzed for each pass to provide supplementary information. To distinguish O mode we have made use of wave

polarization as detected by the RPWS HFR instrument [*Fischer et al.*, 2009; *Ye et al.*, 2010], and we have determined the electron density (as discussed above), since O mode cannot propagate below f_p. The polarization of Z mode for $f_p < f_c$ and $f > f_p$ is right-handed (RH), while for $f < f_p$, the polarization is left-handed [*Benson et al.*, 2006]. This property was observed at times confirming the Z-mode identification. While some whistler mode emission was observed even for $r < 4.5\,R_s$, it seldom extended in frequency above 3 kHz, where virtually all the Z mode was observed. Whistler mode emission typically has a broadband morphology, distinct from the narrowband Z mode, and whistler mode polarization is always RH.

We introduce $\beta_i = f_i/f_{\mathrm{ref}}$, where f_i is the center of the frequency bin, $\Delta\beta_i$, and $f_{\mathrm{ref}} = 5$ kHz. We let $\Delta f = 1$ kHz where 3 kHz $< f_i <$ 8 kHz and $f_i - f_{i-1} = \Delta f$, and $\Delta\beta_i = \beta_i - \beta_{i-1}$. There can be many frequency values within each $\Delta\beta_i$ at each time step, $\Delta\tau$. The wave intensities are proportional to $P_E = E^2 (\mathrm{V}^2/\mathrm{m}^2)$. From the electric spectral density measured in $\mathrm{V}^2/(\mathrm{m}^2\,\mathrm{Hz})$ over a range of frequencies, we determine $E^2(\beta_i)$ (measured in $\mathrm{V}^2/\mathrm{m}^2$), by integration over the frequency channels within $\Delta\beta_i$ for a time step, $\Delta\tau$ (typically 1 min). The sum of these integrations is what we call P_{Ei}. The spacecraft position (r, λ, and LT) at each time step, $\Delta\tau$, is always recorded. To obtain $P_E(\beta)$ we calculate the mean value of P_E within any chosen spatial bin (Δr, $\Delta\lambda$, and ΔLT) by averaging all P_{Ei} within that spatial bin during the total integration time, $T_{\mathrm{total}} = \sum_i \Delta\tau_i$. For a particular Δr, by calculating averages over all values of LT, and all values of λ, we can fit $P_E(\beta)$ to a Gaussian of the form

$$P_E(\beta) = P_o \exp\left\{ -(\beta - \beta_o)^2/w^2 \right\}, \qquad (1)$$

with fitting parameters P_o, β_o, and w (cf., *Glauert and Horne* [2005], *Shprits et al.* [2006], *Glauert et al.* [2014], and others).

We calculate the value of P_E per spectrum, P_{ES}, by performing the sum over all β_i, $\sum_i P_{Ei}$, for each $\Delta\tau$. To obtain P_E for a specific spatial range, we determine the mean of all P_{ES} within that spatial range during the total integration time, T_{total}. As an example, to obtain $P_E(\lambda)$ we calculate the mean values of P_{ES} within a specific Δr for all values of LT and for all values of λ within each bin of latitude, $\Delta\lambda$, then we fit to the functional form

$$P_E(\lambda) = P_o \exp\left\{ -(\lambda - \lambda_o)^2/w^2 \right\}, \qquad (2)$$

Because the magnetic field intensities are seldom above the noise level of the RPWS search coils, we determine the wave magnetic intensity levels by evaluating the cold plasma index of refraction $\eta(f, f_c, f_p)$ [*Stix*, 1992, equation (34)], then we obtain $B = \eta E/c$, where E is the observed electric field intensity evaluated as just outlined. The values of P_B and P_{BS} are defined in a similar fashion as P_E and P_{ES}. We have performed the calculations for an assumed wave normal angle (between the wave vector and the ambient magnetic field) of $\psi = 85°$ and $\psi = 5°$ and found very similar results. We display only the results for $\psi = 85°$. The average index of refraction of the Z mode within a time step, calculated from cold plasma theory, ranged from $\sim 0 < \eta_{\mathrm{avg}} \lesssim 1.4$.

4. Models and Data Constraints

The Z3 zonal harmonic model [*Acuña et al.*, 1983] has been used for the Saturn magnetic field. Since the upper hybrid resonance, $f_{\mathrm{uh}} = \sqrt{f_p^2 + f_c^2}$, where f_p is the local plasma density, is not observed in the low-density regions where we expect Z mode, we have used density obtained from the Langmuir Probe (LP) onboard Cassini [*Wahlund et al.*, 2005]. The floating potential of the LP is used as a proxy to evaluate the electron number density in a tenuous plasma ($< 5\,\mathrm{cm}^{-3}$) [cf. *Morooka et al.*, 2009]. These densities are tabulated in time and are interpolated for this study. However, there are gaps in this data set, where the spacecraft potential is not well known or the density is too high, at which times we interpolate values of the Saturn plasma density using the model of *Persoon et al.* [2013] for Saturn's inner magnetosphere. At high-latitude regions, where no Langmuir Probe data are available and outside the range of the density model, we assume the plasma density, $n_e \ll 1\,\mathrm{cm}^{-3}$, and the index of refraction, $\eta = 1$.

The spectral density values were obtained at Saturn from the radio and plasma wave science (RPWS) instrument [*Gurnett et al.*, 2004], using only the middle-frequency receiver (24 Hz–12 kHz) and high-frequency receiver (HFR) (3.5 kHz–16 MHz). There are three approximately orthogonal electric antennas
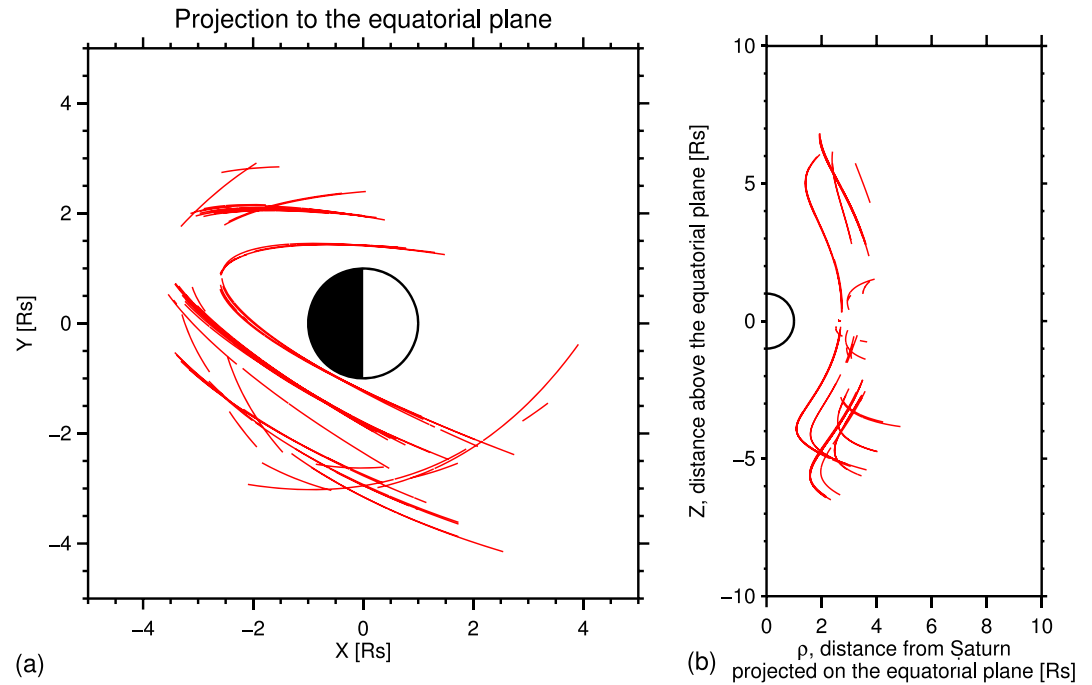
Figure 3. Plots of the orbit segments at times when Cassini RPWS observed Z mode projected onto (a) the equatorial (x-y) plane and (b) the ρ-z plane.

(10 m) and three orthogonal search coils for magnetic measurements. To avoid background noise we set a minimum electric power spectral density $> 10^{-16}\,\mathrm{V}^2/(\mathrm{m}^2\,\mathrm{Hz})$.

5. Data Sampling Times and Locations

The data for the Saturn survey were obtained over approximately 7.5 years from 15 January 2005 to 8 July 2013. In Figure 3 we display plots of the segments of orbits projected onto the equatorial (x-y) plane and the ρ-z plane where Z-mode emission was observed. As expected [cf. *Ye et al.*, 2010] Z mode is observed relatively close to Saturn. Sampling of the region near local noon and afternoon was not complete for the low-perigee orbits, especially those sampling the region inside the Enceladus torus, so no definitive statements can be made about the occurrence of Z mode in this region.

6. Saturn Intensity Surveys

In Figure 4 we display the number of spectra and the average electric intensity per spatial bin in the r-LT plane and summed over all latitudes in the range $0 < |\lambda| < 80°$. These bins are mapped to the equatorial plane. For these plots we have used ΔLT = 1 h and $\Delta r = 1\ R_s$. While there is reasonable sampling from ~18 h $<$ LT $<$ 10 h (counterclockwise), there is a lack of data sampling at small r for ~12 h $<$ LT $\lesssim$ 20 h. Cassini orbits intercepted this region, but they did not do so for $r < 4\ R_s$. In Figure 4a we display the number of spectra of Z mode within each bin during the total survey time, T_{total}. In Figure 4b we display the average Z-mode intensity by averaging all the values of P_{ES} in each spatial bin for the complete survey time. We see relatively high-intensity levels at smaller radial distances for 22 h $<$ LT $<$ 3 h and also for 7 h $<$ LT $\lesssim$ 11 h. In Figure 5 we also bin the data in the r-λ or meridian plane. In Figure 5a we show the number of Z-mode spectra observed in each spatial bin during T_{total}. In Figure 5b we display the Z-mode intensity by averaging the electric intensity within each r-λ bin at all LTs. For this plot we let $\Delta\lambda = 5°$ for $\lambda \leq 10°$ and $\Delta\lambda = 10°$ for $\lambda > 10°$. We see that relatively large intensities are observed for smaller r and $\lambda \lesssim 40°$. The magnetic intensities (nT^2) show a very similar distribution as displayed by the electric intensities in Figures 4 and 5 and are not shown.
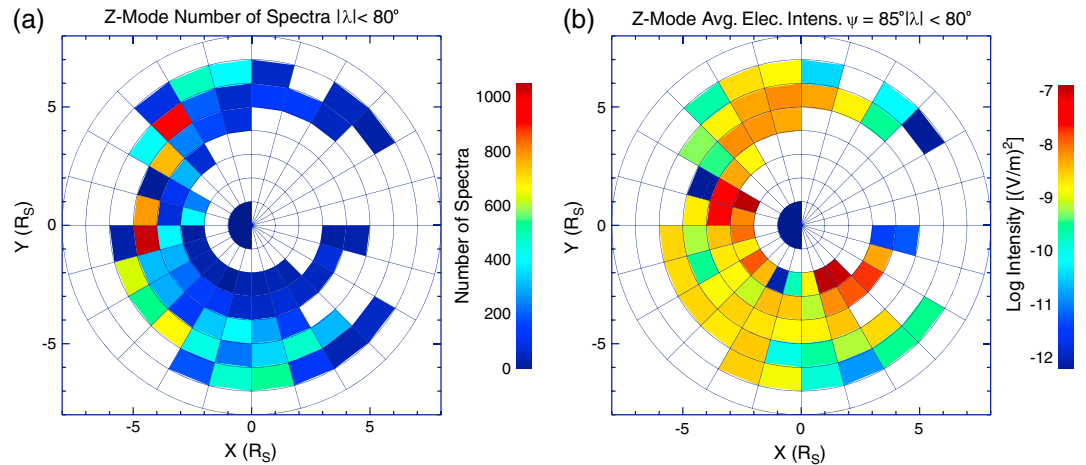
Figure 4. (a) The number of spectra of Z-mode emission observed within each bin of the r-LT plane during the total survey time, T_{total}. The bins (defined in the text) are mapped to the equatorial plane. (b) We display the average Z-mode intensity by averaging all the values of P_{ES} in each spatial bin for the complete survey time. We see relatively high intensity levels at smaller radial distances for 22 h < LT < 3 h and also for 7 h < LT < ~11 h.

7. Fitting the Data

We next greatly expand the bin size and construct fits of average Z-mode intensity using equation (1). For a range of r we obtain the average of P_E and P_B for all spectra within a spatial bin that includes all local times and $|\lambda| < 80°$. Figures 6a and 6b show the results centered at two ranges of r, with $\Delta r = 1\ R_s$, while Figure 6c shows the results averaged over the full range of r, $2\ R_s < r < 7\ R_s$. The values of the fitting parameters are
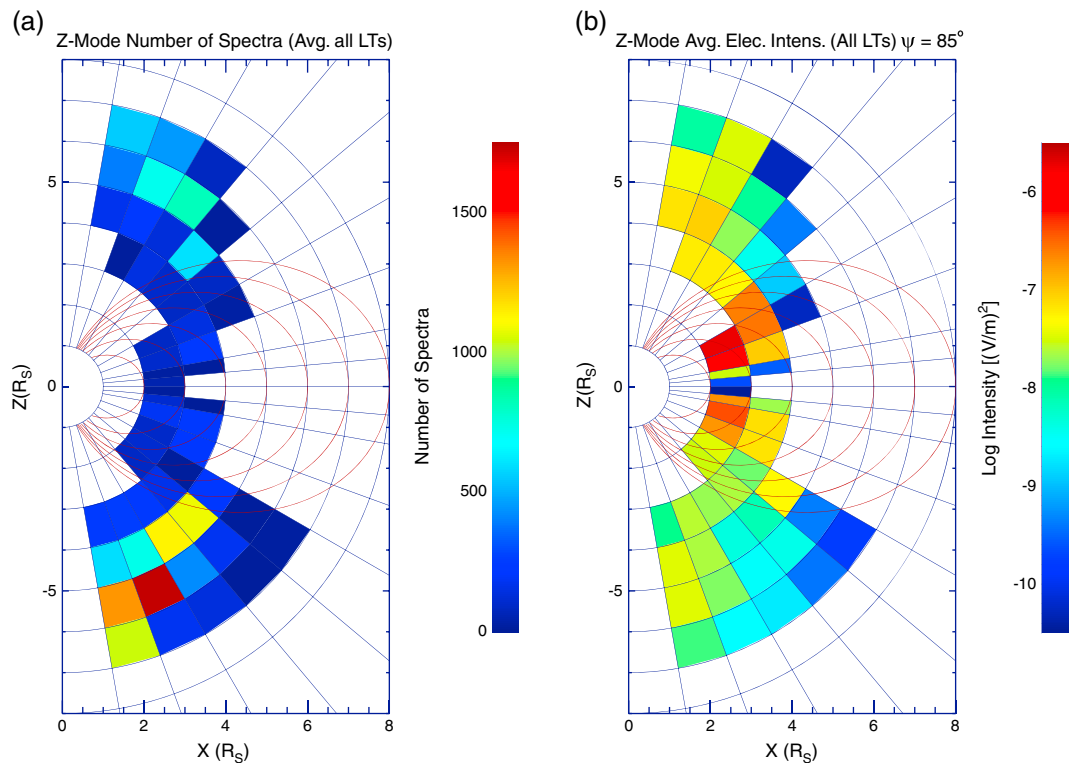

Figure 5. (a) The number of Z-mode spectra observed in each spatial bin of the r-λ or meridian plane during T_{total}. (b) We display the Z-mode average electric field intensity within each r-λ bin (averaging all LTs). Relatively large intensities are observed for smaller r and $\lambda \lesssim 40°$.
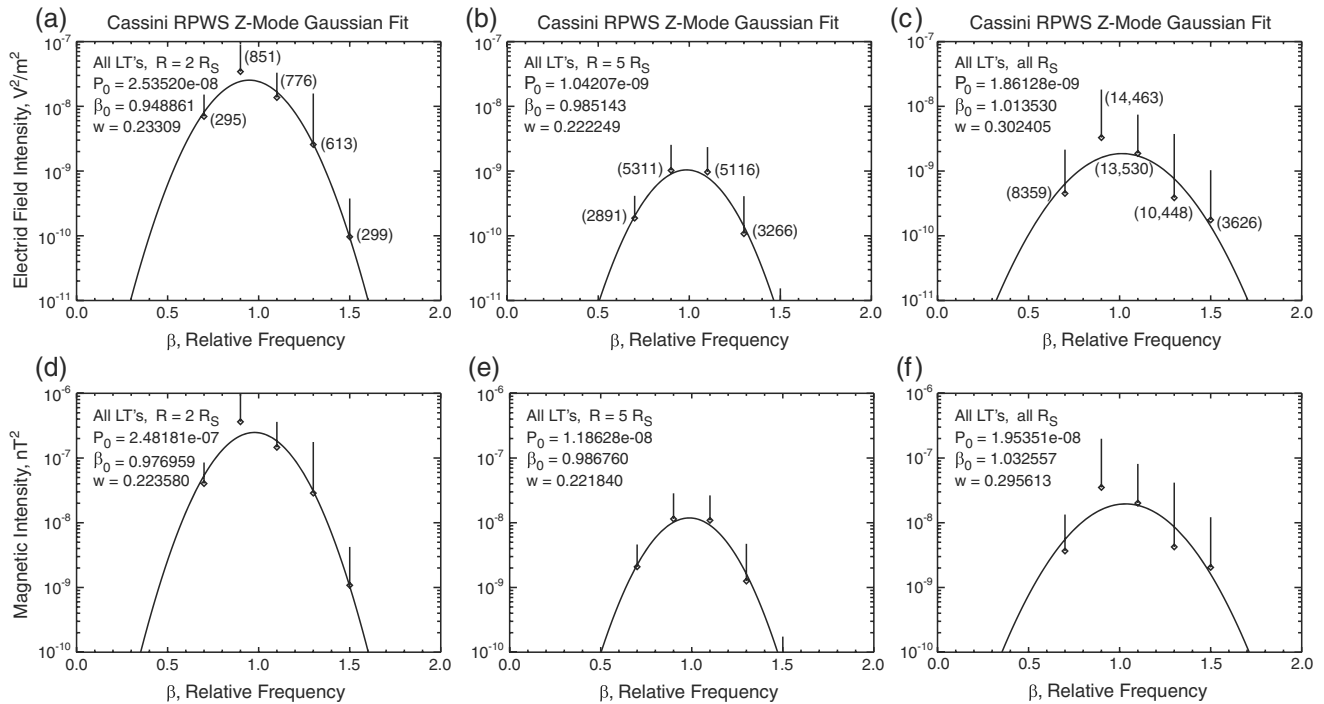
Figure 6. Fits of average Z-mode electric and magnetic intensity versus frequency using equation (1) for an expanded bin size (see text). Results are shown for r centered at (a) $2\,R_s$ and (b) $5\,R_s$ ($\Delta r = 1\,R_s$), while (c) the results averaged over the full range of r, $2\,R_s < r < 7\,R_s$ are also presented. The values of the fitting parameters are listed on each plot. The error bars are determined from the variance of points within the bins, and because of the semilog plot only half of the bar is depicted. (d–f) The results for the magnetic intensity are shown. The number of points within each bin is shown in parentheses on Figures 6a–6c.

listed on each plot. These results are for a wave normal angle of $\psi = 85°$ but are quite similar for $\psi = 5°$. The error bars are determined from the variance of points within the bins, and because of the semilog plot only half of the bar is depicted. Figures 6d–6f show the results for the magnetic intensity. The number of points within each bin is shown in parentheses on Figures 6a–6c.

For each panel of Figure 6 we see a similar morphology, with a peak near $\beta \sim 1$ and a reasonable fit to a Gaussian, but the intensity levels drop rapidly with r. The peak electric intensity, $P_{oE,B}$ ranges from $2.5 \times 10^{-8}\,V^2/m^2$ ($r = 2.5\,R_s$) down to $1.0 \times 10^{-9}\,V^2/m^2$ ($r = 5.5\,R_s$), while the magnetic intensity varies from $2.5 \times 10^{-7}\,nT^2$ ($r = 2.5\,R_s$) down to $1.2 \times 10^{-8}\,nT^2$ ($r = 5.5\,R_s$).

In Figure 7, for two functional forms, we display a least squares fit to the intensity, integrated over frequency, with respect to r. For these fits we have separately averaged P_{ES} and P_{BS} for all LTs and λ for each radial bin. For integer exponents the data can be fit to a sum of polynomials with dominant term r^{-3}, as seen in Figure 7a, while for non integer exponent, the intensity is fit to $r^{-5.0}$ in Figure 7b. The actual points are the "plus" symbols with the number of points given next to the symbol in parentheses (Figure 7a). The same plots for the magnetic field intensity are shown in Figures 7c and 7d, which show a similar but somewhat steeper radial profile.

Next we examine the latitudinal distribution of Z-mode intensity using equation (2). We average the spectral power over a spatial bin that includes all radial distances and all local times and successive bins in $|\lambda|$. In other words the latitude bins in both hemispheres (north and south) are averaged together. The bin size is $\Delta\lambda = 5°$ for $\lambda < 10°$ and $\Delta\lambda = 10°$ for $\lambda > 10°$. The results are displayed in Figure 8, which shows an increase in intensity from the equator until $\lambda = 25°$, where $P_{oE} = 3.874 \times 10^{-8}\,V^2/m^2$ (Figure 8a) and $P_{oB} = 4.25 \times 10^{-7}\,nT^2$ (Figure 8b). After this latitude there is a rapid decrease in intensity. The number of points within each latitude bin is shown in parentheses of Figure 8a. The larger numbers of points for bins for $\lambda \geq 40°$ is due to the slower spacecraft velocity and larger bin size at larger radial distances. We also conduct the binning in latitude by limiting the radial distance to $r < 4\,R_s$ to avoid the region within the dense Enceladus torus. These results are shown for the electric and magnetic intensities in Figures 8b and 8d, respectively, and are similar to those of Figures 8a and 8b, but in all cases the least squares analysis indicates that a Gaussian does not fit
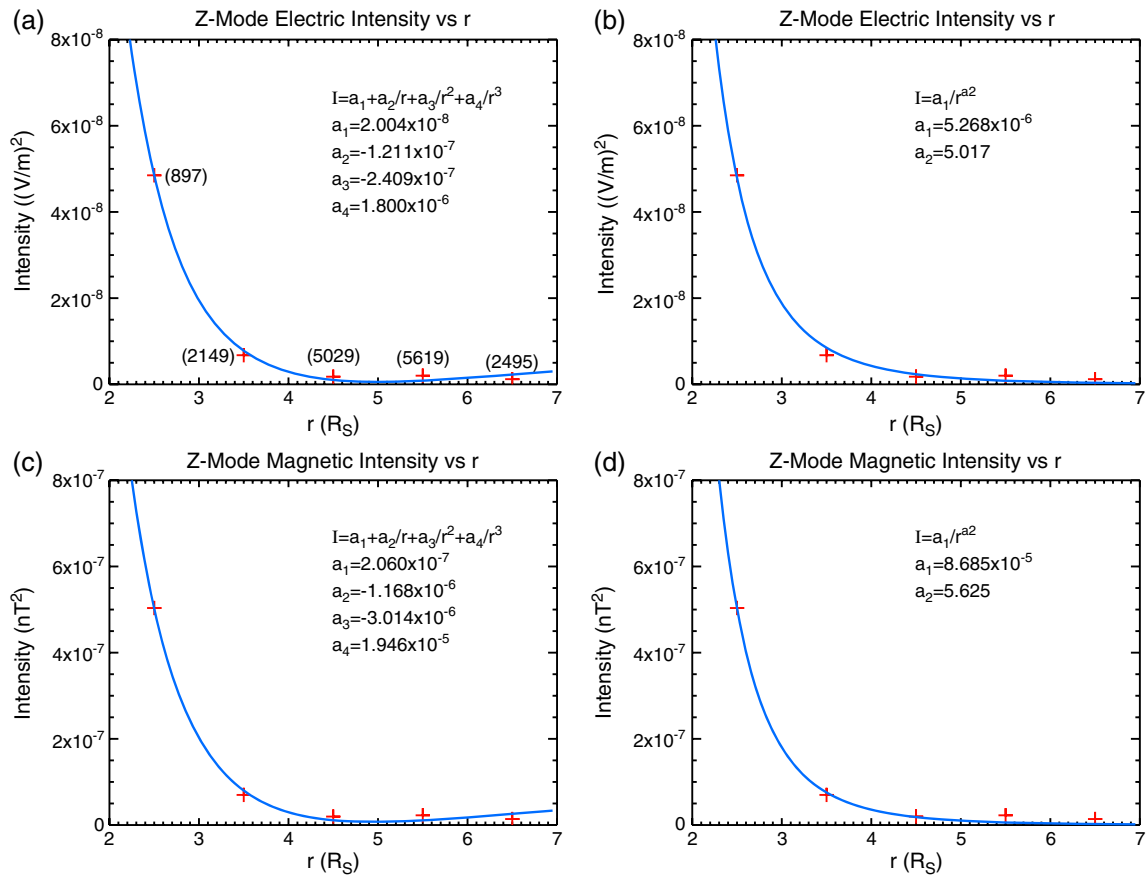
Figure 7. Least squares fit to the average Z-mode intensity, integrated over frequency, with respect to r as described in the text. (a) For integer exponents the electric field data are fit to a sum of polynomials with dominant term r^{-3}, while (b) for noninteger exponent, the intensity is fit to $r^{-5.0}$. The actual points are the plus symbols with the number of points given next to the symbol in parentheses (Figure 7a). The same plots for the magnetic field intensity are shown in Figures 7c and 7d, which display a similar radial profile.

the data well. We therefore fit the points for $r < 4\,R_s$ and $\lambda \leq 25°$ to a parabola ($I = a_1\,\lambda^2 + a_2\,\lambda + a_3$) as shown in Figures 9a and 9b for the electric and magnetic Z-mode intensities, respectively. The fitting parameters for these functional fits are listed on the plots, with λ measured in degrees.

8. Summary and Conclusions

Z-mode emission is believed to be important in the diffusive scattering and resonant acceleration of electrons. At Saturn, Z-mode emission is observed primarily as 5 kHz narrowband (NB) emission [cf. *Ye et al.*, 2010]. The higher-frequency NB emissions (20 kHz NB) probably contain a component of Z mode but are also frequently (and perhaps dominantly) O mode. We have presented a survey of the intensity of the 5 kHz Z-mode NB emission in the Saturn magnetosphere as a function of frequency, r, λ, and LT. Z-mode emission is observed predominantly in the low-density region inside (near to Saturn) the inner edge of the Enceladus plasma torus at lower latitudes and at higher latitudes extending to about 7 R_s where $f_c/f_p > 1$. This region of the Saturn magnetosphere has not been completely sampled by the Cassini spacecraft to date, particularly near the range of 12 h $\lesssim$ LT $\lesssim$ 18 h. We have adequate sampling, however, to indicate that Z mode is often observed at electric spectral density levels that are comparable to chorus emission, while the magnetic intensity levels of Z mode are probably more than 2 orders of magnitude lower than chorus [cf. *Hospodarsky et al.*, 2012; *Menietti et al.*, 2014]. To estimate an emission occurrence rate we define the sampling time of Z-mode emissions as the time the spacecraft spent in regions where Z-mode emission can propagate. This, as discussed above, is the general region inside the Enceladus plasma density torus where $f_p/f_c < 1$ and $f_z < f < f_{uhr}$. The total number of hours sampled on approximately 40 distinct passes is estimated to be ~352,
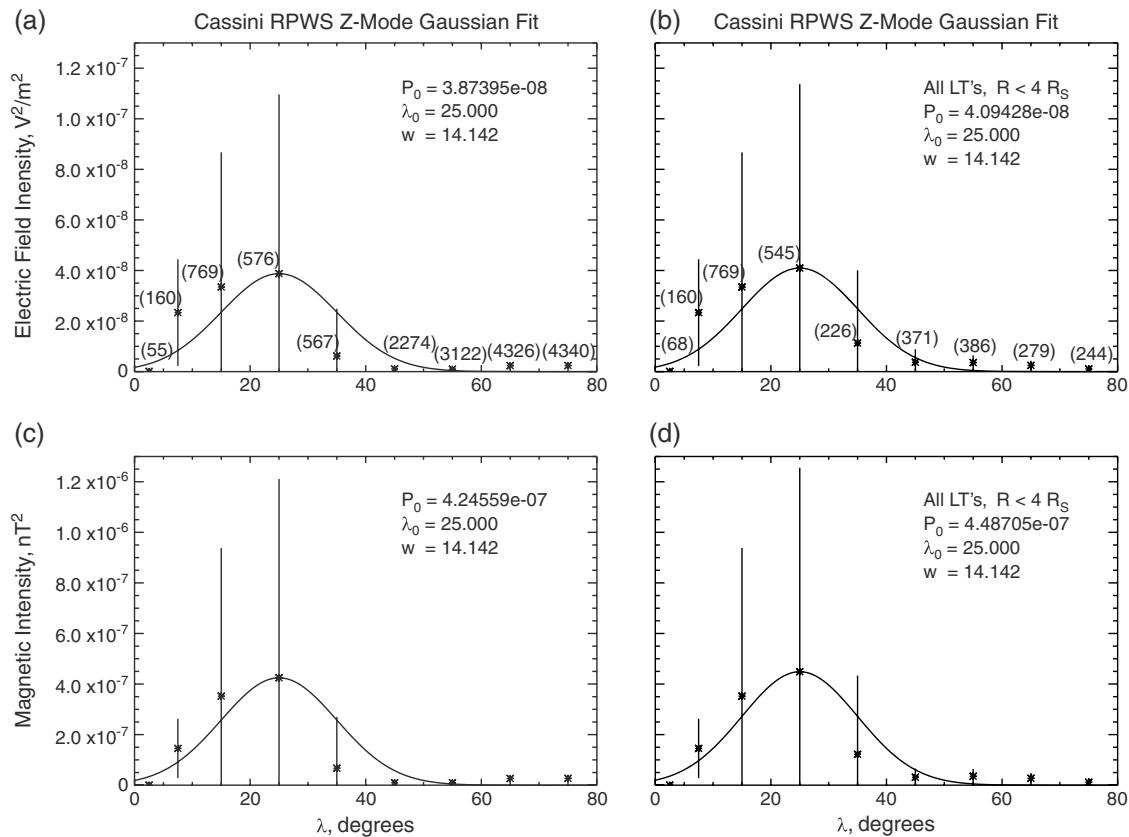
Figure 8. Average Z-mode intensity versus latitude using equation (2). The latitude bins in both hemispheres (north and south) are averaged together (see text for details). There is an increase in intensity from the equator until $\lambda = 25°$, where (a) $P_{oE} = 3.874 \times 10^{-8}$ V²/m² and (c) $P_{oB} = 4.246 \times 10^{-7}$ nT²°s. After this latitude there is a rapid decrease in intensity. The number of points within each latitude bin is shown in parentheses in Figure 8a. (b and d) The results for $r > 4\,R_s$ are shown and are quite similar to those for all R_s, but the points of Figure 8 are not fit well by a Gaussian.

while the total hours of observed Z-mode emission in the frequency range ~3 kHz $< f <$ ~8 kHz are 171.7 h, which is a ratio of 0.487. We note that the sampling time is much smaller than the total time of data analyzed, which is thousands of hours.

We have computed least squares parametric fits of the Z-mode intensity levels as a function of the above-mentioned parameters, which will be useful in modeling the wave-particle interactions and consequent electron acceleration. The Z-mode intensity is strongest at radial distances nearest to Saturn and at a latitude near 25°. We have investigated the frequency range ~3 KHz to ~8 kHz and found that the maximum intensity is quite near 5 kHz. The radial profile of the intensity shows a moderate increase from the equator to ~25° followed by a steep decline. This implies a source region that may be confined to the inner edge of the Enceladus torus as shown in the diagram (Figure 10). In this figure we show the Cassini trajectory on day 167/20:00 to 168/16:00 of 2008. The hours of day are shown along the satellite path. On this orbit Cassini RPWS observed moderate (brown hashing) to intense (green hashing) Z mode at periods along the trajectory. The Z-mode observations for this time period are those discussed by *Ye et al.* [2010] (their Figure 10) and *Gu et al.* [2013] (their Figure 1) and are among the most intense observed in the survey. Overplotted on Figure 10 are the electron density contours [*Persoon et al.*, 2013] for the Enceladus torus. Note that the most intense Z mode is observed above the equator near the inner edge of the torus. Measurements of the wave normal angle are not possible using the Cassini waveform receiver (with two electric and three magnetic antennas), because the frequency range of the instrument extends only to ~2.5 kHz. It is conceivable, based on Figure 10, that Z-mode source regions located near the inner edge of the Enceladus torus could be observed by Cassini for a range of wave normal angles 90° $< \psi <$ 180°. Using RPWS two-antenna direction finding analysis tools (cf. *Ye et al.* [2010] for details of this technique), we have determined that the source region of the Z mode observed in the time intervals 03:00 to 04:00 is in
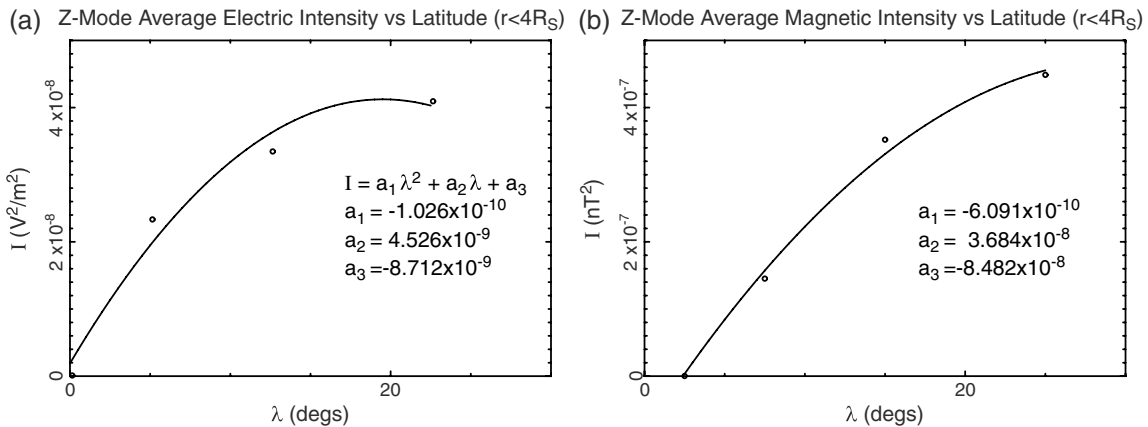
Figure 9. Improved fits of Z-mode intensity versus latitude using polynomial functions. For the points for $\lambda \leq 25°$ the fit is to a parabola ($I = a_1 \lambda^2 + a_2 \lambda + a_3$). The (a) electric and (b) magnetic Z-mode intensities are shown, and the fitting parameters for these functional fits are listed.

the direction of the Enceladus torus (indicated by the arrows and red hashing in Figure 10). It must be remembered, however, that the emission is trapped plasma waves and is therefore probably subject to strong refraction near the source region.
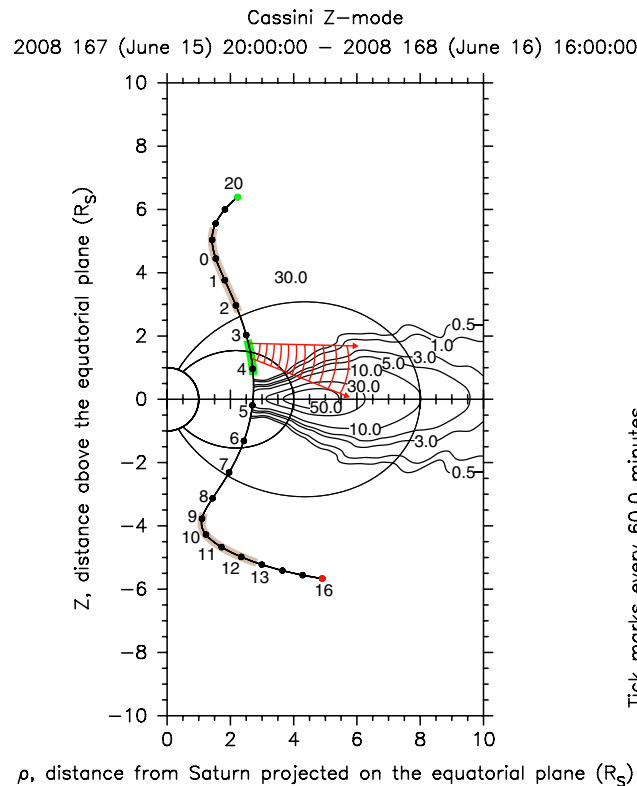

Figure 10. Cassini trajectory on day 167/20:00 to 168/16:00 of 2008. The hours of day are shown along the satellite path. Cassini RPWS observed moderate (brown hashing) to intense (green hashing) Z mode at periods along the trajectory. The Z-mode observations for this time period are among the most intense observed in the survey. Overplotted are the electron density contours [*Persoon et al.*, 2013] for the Enceladus torus. Note that the most intense Z mode is observed above the equator near the inner edge of the torus. The red hashing indicates the calculated direction to the source region during the time period 03:00 to 04:00.

The survey indicates that the strongest Z-mode intensities occur at the smallest sampled radial distances, $r < 3 R_s$, and at latitudes off the equatorial plane. This region overlaps the Saturn G-ring, which is between about 2.75 R_s and 2.9 and not the E-ring where the observations of dust particles associated with Enceladus have been reported [cf. *Kurth et al.*, 2006; *Wahlund et al.*, 2009; *Morooka et al.*, 2011].

The source mechanism for generating the 5 kHz emission is not yet known and should be pursued. The intensity of the Z-mode emission suggests an instability. The possibility of eigenmode trapping in density enhancements in Saturn's inner magnetosphere in regions of $f_p/f_c < 1$ [cf *Yoon et al.*, 2000; *Menietti et al.*, 2007] seems to be precluded by the absence of fine structure in the data, and the consistency of emission centered very near 5 kHz. We conclude that Z-mode wave-particle interactions may make a significant contribution to electron acceleration in the inner magnetosphere of Saturn accelerating electrons up to MeV energies, thus supplementing chorus-generated acceleration at larger L shells [*Menietti et al.*, 2014]. At present observations suggest that chorus waves at Saturn are weak compared to those at Jupiter and Earth, and while chorus has been shown to be very important for the formation of the radiation belts

at Earth [*Horne et al.*, 2005; *Shprits et al.*, 2006] and Jupiter [*Horne et al.*, 2008; *Woodfield et al.*, 2013, 2014], it seems unlikely that they are responsible for the formation of the radiation belts at Saturn [*Shprits et al.*, 2012]. However, *Z*-mode waves appear to be strong and can resonate with electrons at MeV energy values [*Gu et al.*, 2013]. They could therefore provide an important source of electron acceleration contributing to the radiation belts at Saturn. Their effectiveness has yet to be established. The future trajectories of the Cassini spacecraft during the F-ring Orbits Mission will be an excellent opportunity to comprehensively observe *Z*-mode emission in the inner magnetosphere of Saturn, inside the orbit of Enceladus.

References

Acuña, M. H., J. E. P. Connerney, and N. F. Ness (1983), The Z₃ zonal harmonic model of Saturn's magnetic field: Analyses and implications, *J. Geophys. Res.*, *88*(A11), 8771–8778, doi:10.1029/JA088iA11p08771.

Albert, J. M. (2007), Refractive index and wavenumber properties for cyclotron resonant quasilinear diffusion by cold plasma waves, *Phys. Plasmas*, *14*, 072901, doi:10.1063/1.2744363.

Benson, R. F., P. A. Webb, J. L. Green, D. L. Carpenter, V. S. Sonwalkar, H. G. James, and B. W. Reinisch (2006), Active wave experiments in space plasmas: The Z Mode, in *Geospace Electromagnetic Waves and Radiation*, edited by J. W. LaBelle and R. A. Treumann, pp. 3–35, Springer, Berlin, doi:10.1007/3-540-33203-0_1.

Farrell, W. M., W. S. Kurth, M. L. Kaiser, M. D. Desch, D. A. Gurnett, and P. Canu (2005), Narrowband Z-mode emissions interior to Saturn's plasma torus, *J. Geophys. Res.*, *110*, A10204, doi:10.1029/2005JA011102.

Fischer, G., B. Cecconi, L. Lamy, S.-Y. Ye, U. Taubenschuss, W. Macher, P. Zarka, W. S. Kurth, and D. A. Gurnett (2009), Elliptical polarization of Saturn Kilometric Radiation observed from high latitudes, *J. Geophys. Res.*, *114*, A08216, doi:10.1029/2009JA014176.

Glauert, S. A., and R. B. Horne (2005), Calculation of pitch angle and energy diffusion coefficients with the PADIE code, *J. Geophys. Res.*, *110*, A04206, doi:10.1029/2004JA010851.

Glauert, S. A., R. B. Horne, and N. P. Meredith (2014), Three-dimensional electron radiation belt simulations using the BAS Radiation Belt Model with new diffusion models for chorus, plasmaspheric hiss, and lightning-generated whistlers, *J. Geophys. Res. Space Physics*, *119*, 268–289, doi:10.1002/2013JA019281.

Gu, X., R. M. Thorne, B. Ni, and S.-Y. Ye (2013), Resonant diffusion of energetic electrons by narrowband Z mode waves in Saturn's inner magnetosphere, *Geophys. Res. Lett.*, *40*, 255–261, doi:10.1029/2012GL054330.

Gurnett, D. A., et al. (2004), The Cassini radio and plasma wave investigation, *Space Sci. Rev.*, *114*, 395–463, doi:10.1007/s11214-004-1434-0.

Horne, R. B., and R. M. Thorne (1998), Potential waves for relativistic electron scattering and stochastic acceleration during magnetic storms, *Geophys. Res. Lett.*, *25*(15), 3011–3014, doi:10.1029/98GL01002.

Horne, R. B., et al. (2005), Wave acceleration of electrons in the Van Allen radiation belts, *Nat. Lett.*, *437/8*, 227–229, doi:10.1038/nature03939.

Horne, R. B., R. M. Thorne, S. A. Glauert, J. D. Menietti, Y. Y. Shprits, and D. A. Gurnett (2008), Gyro-resonant electron acceleration at Jupiter, *Nat. Phys.*, *4*, 301–304, doi:10.1038/nphys897.

Hospodarsky, G. B., K. Sigsbee, J. S. Leisner, J. D. Menietti, W. S. Kurth, D. A. Gurnett, C. A. Kletzing, and O. Santolík (2012), Plasma wave observations at Earth, Jupiter, and Saturn, in *Dynamics of the Earth's Radiation Belts and Inner Magnetosphere*, edited by D. Summers et al., pp. 415–430, AGU, Washington, D. C., doi:10.1029/2012GM001342.

Kurth, W. S., T. F. Averkamp, D. A. Gurnett, and Z. Wang (2006), Cassini RPWS observations of dust in Saturn's E Ring, *Planet. Space Sci.*, *54*, 988–998, doi:10.1016/j.pss.2006.05.011.

Menietti, J. D., P. H. Yoon, and D. A. Gurnett (2007), Possible eigenmode trapping in density enhancements in Saturn's inner magnetosphere, *Geophys. Res. Lett.*, *34*, L04103, doi:10.1029/2006GL028647.

Menietti, J. D., Y. Y. Shprits, R. B. Horne, E. E. Woodfield, G. B. Hospodarsky, and D. A. Gurnett (2012), Chorus, ECH, and Z mode emissions observed at Jupiter and Saturn and possible electron acceleration, *J. Geophys. Res.*, *117*, A12214, doi:10.1029/2012JA018187.

Menietti, J. D., T. F. Averkamp, J. B. Groene, R. B. Horne, Y. Y. Shprits, E. E. Woodfield, G. B. Hospodarsky, and D. A. Gurnett (2014), Survey analysis of chorus intensity at Saturn, *J. Geophys. Res. Space Physics*, *119*, 8415–8425, doi:10.1002/2014JA020523.

Morooka, M. W., et al. (2009), The electron density of Saturn's magnetosphere, *Ann. Geophys.*, *27*, 2971–2991, doi:10.5194/angeo-27-2971-2009.

Morooka, M. W., J.-E. Wahlund, A. I. Eriksson, W. M. Farrell, D. A. Gurnett, W. S. Kurth, A. M. Persoon, M. Shafiq, M. André, and M. K. G. Holmberg (2011), Dusty plasma in the vicinity of Enceladus, *J. Geophys. Res.*, *116*, A12221, doi:10.1029/2011JA017038.

Persoon, A. M., D. A. Gurnett, J. S. Leisner, W. S. Kurth, J. B. Groene, and J. B. Faden (2013), The plasma density distribution in the inner region of Saturn's magnetosphere, *J. Geophys. Res. Space Physics*, *118*, 2970–2974, doi:10.1002/jgra.50182.

Shprits, Y. Y., R. M. Thorne, R. B. Horne, and D. Summers (2006), Bounce-averaged diffusion coefficients for field-aligned chorus waves, *J. Geophys. Res.*, *111*, A10225, doi:10.1029/2006JA011725.

Shprits, Y. Y., J. D. Menietti, X. Gu, K. C. Kim, and R. B. Horne (2012), Gyroresonant interactions between the radiation belt electrons and whistler mode chorus waves in the radiation environments of Earth, Jupiter, and Saturn: A comparative study, *J. Geophys. Res.*, *117*, A11216, doi:10.1029/2012JA018031.

Stix, T. H. (1992), *Waves in Plasmas*, p. 9, American Institute of Physics, New York.

Wahlund J.-E., et al. (2005), The inner magnetosphere of Saturn: Cassini RPWS cold plasma results from the first encounter, *Geophys. Res. Lett.*, *32*, L20S09, doi:10.1029/2005GL022699.

Wahlund, J.-E., et al. (2009), Detection of dusty plasma near the E-ring of Saturn, *Planet. Space Sci.*, *57*, 1795–1806, doi:10.1016/j.pss.2009.03.011.

Woodfield, E. E., R. B. Horne, S. A. Glauert, J. D. Menietti, and Y. Y. Shprits (2013), Electron acceleration at Jupiter: Input from cyclotron-resonant interaction with whistler-mode chorus waves, *Ann. Geophys.*, *31*, 1619–1630, doi:10.5194/angeo-31-1619-2013.

Woodfield, E. E., R. B. Horne, S. A. Glauert, J. D. Menietti, and Y. Y. Shprits (2014), The origin of Jupiter's outer radiation belt, *J. Geophys. Res. Space Physics*, *119*, 3490–3502, doi:10.1002/2014JA019891.

Xiao, F., S. Zhang, Z. Su, Z. He, and L. Tang (2012), Rapid acceleration of radiation belt energetic electrons by Z-mode waves, *Geophys. Res. Lett.*, *39*, L03103, doi:10.1029/2011GL050625.

Ye, S.-Y., D. A. Gurnett, G. Fischer, B. Cecconi, J. D. Menietti, W. S. Kurth, Z. Wang, G. B. Hospodarsky, P. Zarka, and A. Lecacheux (2009), Source locations of narrowband radio emissions detected at Saturn, *J. Geophys. Res.*, *114*, A06219, doi:10.1029/2008JA013855.

Ye, S.-Y., J. D. Menietti, G. Fischer, Z. Wang, B. Cecconi, D. A. Gurnett, and W. S. Kurth (2010), Z mode waves as the source of Saturn narrowband radio emissions, *J. Geophys. Res.*, *115*, A08228, doi:10.1029/2009JA015167.

Yoon, P. H., A. T. Weatherwax, and J. LaBelle (2000), Discrete electrostatic eigenmodes associated with ionospheric density structure: Generation of auroral roar fine frequency structure, *J. Geophys. Res.*, *105*(A12), 27,589–27,596, doi:10.1029/2000JA000140.